Proceedings of IMECE 2002:
2002 ASME International Mechanical Engineering Congress
November 17-22, 2002, New Orleans, LA

IMECE2002-33873

EMBEDDED ULTRASONIC STRUCTURAL RADAR WITH PIEZOELECTRIC WAFER ACTIVE SENSORS FOR THE NDE OF THIN-WALL STRUCTURES

Victor Giurgiutiu
Mechanical Engineering Department, University of South Carolina Columbia, SC 29208, 803-777-8018,
victorg@sc.edu

Jingjing Bao
Mechanical Engineering Department, University of South Carolina, Columbia, SC 29208, 803-777-1535;
jbao0000@engr.sc.edu

ABSTRACT

Embedded-ultrasonics structural radar (EUSR) is a new concept and methodology for in-situ nondestructive evaluation (NDE) and structural health monitoring (SHM) of thin-wall structures. EUSR consists (a) an array of piezoelectric wafer active sensors (PWAS) embedded into the structure; and (b) electronic modules for signal transmission/reception, processing, and interpretation. EUSR utilizes guided elastic waves (Lamb waves) generated omnidirectionally into the thin-wall structure by surface-mounted permanently-attached PWAS. The paper starts with the general concepts of the EUSR algorithm: transmission beamforming, reception beamforming, and time of fight determination. Next, details of the Lamb wave generation with PWAS, verification of group-velocity dispersion curves, identification of optimal excitation frequency, and confirmation of wave front omnidirectionality are discussed. In the third part of the paper, the actual implementation of the EUSR method in a proof-of-concept demonstration is presented. The construction of the PWAS phased array is described, and detection of cracks located broadside and offside of the PWAS array is illustrated. The method is shown to be easy to use through a visually interactive LabView™ interface. Very good detection accuracy is observed. Though the proof-of-concept experiments presented in this paper were illustrated on metallic structures, the EUSR concept works just as well on composite and hybrid structures.

INTRODUCTION

Ultrasonic inspection of thin wall structures (e.g., aircraft shells, storage tanks, large pipes, etc.) is a time consuming operation that requires meticulous through-the-thickness C-scans of large areas. One method of increasing the efficiency of such inspection is to utilize guided Lamb waves instead of the conventional pressure waves [1-4]. Guided waves propagate inside thin-wall plates and shallow shells parallel to the mid-surface. They can travel at large distances with very little amplitude loss. Traditionally, guided waves have been generated by impinging the plate obliquely with a tone-burst from a relatively large ultrasonic transducer [5]. Deutsch et al. [6] demonstrated phased array for the Lamb wave inspection of thin plates utilizing wedge-coupled conventional ultrasonic transducers and elaborated electronics. Steering and focusing of the Lamb waves beam was demonstrated. Wide-area ultrasonic inspection of aircraft, missiles, pressure vessels, oil tanks, pipelines, etc. was advocated. Another way to generate guided waves is with a comb transducer, which consists of a linear array of tapping transducers that are fired consecutively. With this method, the generated waves tend to stay in a narrow beam aligned with the array axis [7-9].

Though the Lamb-wave phased array methods are promising, the fact that they are based on conventional ultrasonic transducers may make them unsuitable for structural health monitoring (SHM) applications. Three main reasons are apparent: (i) size and weight, (ii) cost, and (iii) principle of operation. Because conventional ultrasonic transducers are bulky and expensive, it seems impractical and costly to conceive using them in a SHM system permanently installed in an aircraft structure and having sufficient transducers to achieve the required structural coverage. However, this is possible with a different class of transducers, the piezoelectric wafer active sensors (PWAS) [10]. The PWAS, which are both small and inexpensive, have the potential for in-situ ultrasonics through inexpensive and unobtrusive deployment as sensor arrays [11]. Early work has shown that PWAS devices can successfully generate Lamb waves in thin-wall composite structures [12-14] as well as in metallic structures [15]. The present paper shows that these devices can be also utilized as phased arrays, in the form of the *embedded-ultrasonics structural radar* (EUSR) [16]. EUSR concept consists of: (a) a PWAS array embedded onto the structure; and (b) electronic modules for signal transmission/reception, processing, and interpretation. Once the beam steering and focusing has been established, the detection of internal flaws is done with the pulse-echo method. Due to its low cost, small size, and unobtrusiveness, the EUSR concept based on PWAS transducers seems better suited for in-situ SHM of thin-wall structures than conventional ultrasonic transducers. EUSR was developed as an extension of our previous work on PWAS-generated Lamb wave SHM [16]. Figure 1 presents the general concept of such a system being installed on a large aircraft. This paper starts with the general principles of the EUSR concept, then describes developmental work on PWAS-generated Lamb waves, and ends with the presentation of the EUSR system design, calibration, and experimental testing.

Copyright © 2002 by ASME

Downloaded From: https://proceedings.asmedigitalcollection.asme.org on 06/28/2019 Terms of Use: http://www.asme.org/about-asme/terms-of-use

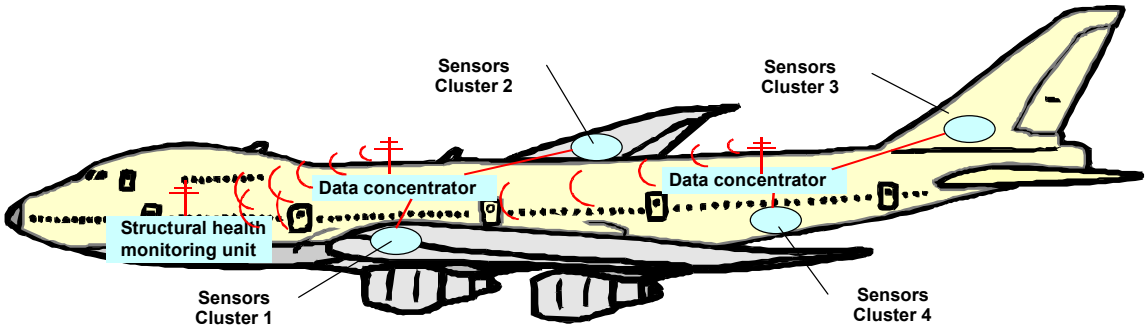

Figure 1 General concept of a sensor-array aircraft structural health monitoring system [16]

EMBEDDED-ULTRASONIC STRUCTURAL RADAR (EUSR)

The embedded ultrasonic structural radar (EUSR) is a concept that utilizes the phased-array radar principles and ultrasonic guided waves (Lamb waves) to scan large surface areas of thin-wall structures for the detection of cracks and corrosion defects [17]. In the EUSR concept, the guided Lamb waves are generated with surface-mounted piezoelectric wafer active sensors (PWAS). The guided Lamb waves have the property of staying confined inside the walls of a thin-wall structure. Hence, they can travel over large distances with little attenuation. In addition, they can also travel inside curved walls with shallow curvature. Thus, the target location is described by the radial position, R, and the azimuth angle, ϕ. In conventional radars, the radar dish sweeps the horizon with a search beam that registers an echo when a target is detected. The phased-array radar replaces the rotating radar dish with an array of M active sensors that are electronically switched such as to generate a virtual sweep beam. The EUSR algorithm is adopted from the beamforming process currently used in phased-array radar applications. Consider a PWAS array as presented in Figure 2a. Each element in the PWAS array plays the role of both transmitter and receiver. A methodology is designed to change the role of each PWAS in a round robin fashion. The responses of the structure to all the excitation signals are collected. By applying the EUSR algorithm, an appropriate delay is applied to each signal in the data set to make them all focus on a direction denoted by angle ϕ. When this angle ϕ is changed from 0 to 180 degrees, a virtual scanning beam is formed and a large area of the structure can be interrogated. Lamb waves can exist in a number of dispersive modes. However, through smoothed tone-burst excitation and frequency tuning, it is possible to confine the excitation to a particular Lamb wave mode, of carrier frequency F_c, wave speed c, and wave length $\lambda = c/F_c$. Hence, the smoothed tone-burst signal generated by one PWAS is assumed of the form:

$$s_T(t) = s_0(t)\cos 2\pi F_c t \ , \ 0 < t < t_p \qquad (1)$$

where $s_0(t)$ is a short-duration smoothing window that is applied to the carrier signal of frequency F_c between 0 and t_p. As in conventional phased array radar [18], we assume a uniform linear array of M active sensors (PWAS), with each PWAS acting as a pointwise omni-directional transmitter and receiver. The PWAS in the array are spaced at the distance d, which is assumed much smaller than the distance r to a generic, far-distance point, P. Since $d << r$, the rays joining the sensors with the point P can be assimilated with a parallel fascicle, of azimuth ϕ (Figure 2a). Because of the array spacing, the distance between one PWAS and the generic point P will be different from the distance between another PWAS and P. For the m-th PWAS, the distance will be shorted by $m(d\cos\phi)$. If all the PWAS are fired simultaneously, the signal from the m-th PWAS will arrive at P quicker by $\Delta_m(\phi) = m(d\cos\phi)/c$. If the PWAS are not fired simultaneously, but with some individual delays, δ_m, m = 0,1,…, M-1, then the total signal received at point P will be:

$$s_P(t) = \frac{1}{r}\sum_{m=0}^{M-1} s_T\left(t - \frac{r}{c} + \Delta_m(\phi) - \delta_m\right) \qquad (2)$$

where $1/r$ represent the decrease in the wave amplitude due to the omni-directional 2-D radiation, and r/c is the delay due to the travel distance between the reference PWAS (m = 0) and the point P. (wave-energy conservation, i.e., no dissipation, is assumed.)

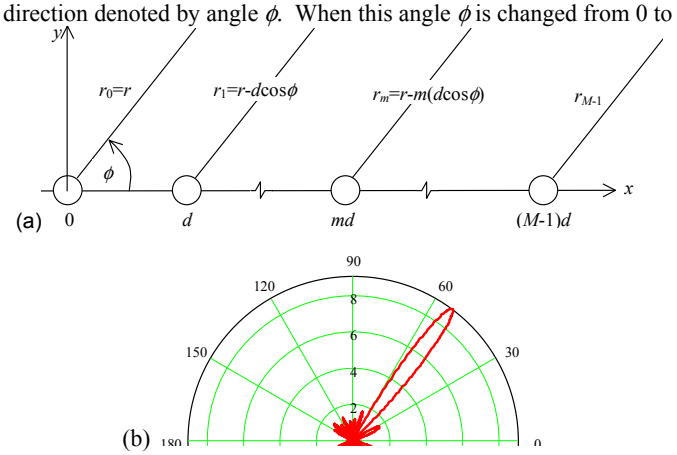

Figure 2 (a) uniform linear array of M omni-directional active sensors spaced at pitch d; (b) calculated beamforming pattern for a 9-sensor array (spacing l = λ/2) with 53-deg target azimuth

TRANSMITTER BEAMFORMING

Beamforming at angle ϕ_0 with an array of M omni-directional sensors is based on the principles of constructive interference in the fascicle of parallel rays emanating from the array. The simplest way of achieving constructive interferences, is to have $\delta_m = m\Delta(\phi)$, such that Equation (2) becomes

$$s_P(t) = M \cdot \frac{1}{r} s_T\left(t - \frac{r}{c}\right) \qquad (3)$$

i.e. an M times increase in the signal strength with respect to a simple sensor. This leads directly to the beamforming principle, i.e., if $\delta_m = m\frac{d}{c}\cos(\phi_0)$, and since $\Delta_m = m\frac{d}{c}\cos(\phi)$, then constructive interference (beamforming) takes place when $\cos(\phi) = \cos(\phi_0)$, i.e. at

Copyright © 2002 by ASME

Downloaded From: https://proceedings.asmedigitalcollection.asme.org on 06/28/2019 Terms of Use: http://www.asme.org/about-asme/terms-of-use

angles $\phi = \phi_0$ and $\phi = -\phi_0$. Thus, the forming of a beam at angles ϕ_0 and $-\phi_0$ is achieved through delays in the firing of the sensors in the array. Figure 2b shows the beam forming pattern for $\phi_0 = 53$ deg.

RECEIVER BEAMFORMING

The receiver beamforming principles are reciprocal to those of the transmitter beamforming. If the point P is an omni-directional source at azimuth ϕ_0, then the signals received at the m-th sensor will arrive quicker by $m\Delta_0(\phi) = m(d\cos\phi_0)/c$. Hence, we can synchronize the signals received at all the sensors by delaying them by $\delta_m(\phi_0) = m\frac{d}{c}\cos(\phi_0)$

PHASED-ARRAY PULSE-ECHO

Assume that a target exists at azimuth ϕ_0 and distance R. The transmitter beamformer is sweeping the azimuth in increasing angles ϕ and receives an echo when $\phi = \phi_0$. The echo will be received on all sensors, but the signals will not be in synch. To synchronize the sensors signals, the delays $\delta_m(\phi_0) = m\frac{d}{c}\cos(\phi_0)$ need to be applied. The process is as follows. The signal send by the transmitter beamformer is an M times boost or the original signal:

$$s_{\mathrm{P}}(t) = \frac{M}{R} s_{\mathrm{T}}\left(t - \frac{2R}{c}\right) \tag{4}$$

At the target, the signal is backscattered with a backscatter coefficient, A. Hence, the signal received at each sensor will be $\frac{A \cdot M}{R^2} s_{\mathrm{T}}\left(t - \frac{2R}{c} + \Delta_m(\phi)\right)$. The receiver beamformer assembles the signals from all the sensors with the appropriate time delays, i.e.,

$$s_{\mathrm{R}}(t) = \frac{A \cdot M}{R^2} \sum_{m=0}^{M-1} s_{\mathrm{T}}\left(t - \frac{2R}{c} + \Delta_m(\phi) - \delta_m\right) \tag{5}$$

Constructive interference between the received signals is achieved when $\delta_m = m\frac{d}{c}\cos(\phi_0)$. Thus, the assembled receive signal will be again boosted M times, with respect to the individual sensors, i.e.,

$$s_{\mathrm{R}}(t) = \frac{A \cdot M^2}{R^2} \sum_{m=0}^{M-1} s_{\mathrm{T}}\left(t - \frac{2R}{c}\right) \tag{6}$$

The time delay between the receive signal, $s_{\mathrm{R}}(t)$ and the transmit signal $s_{\mathrm{T}}(t)$, is

$$\tau = \frac{2R}{c} \tag{7}$$

Measurement of the time delay τ observed in $s_{\mathrm{R}}(t)$ allows one to calculate the target range, $R = c\tau/2$.

PRACTICAL IMPLEMENTATION OF THE EUSR ALGORITHM

The practical implementation of the signal generation and collection algorithms is described next: In a round-robin fashion, one active sensor at a time is activated as transmitter. The reflected signals are received at all the sensors. The activated sensor acts in pulse-echo mode, i.e. as both transmitter and receiver, the other sensors act as passive sensors. Thus, an M x M matrix of signal primitives is generated (Table 1). The signal primitives are assembled into synthetic beamforming responses using the synthetic beamformer algorithm given by Equations (2) and (3). The delays, δ_i, are selected in such a way as to steer the interrogation beam at a certain angle, ϕ_0. The synthetic-beam sensor responses, $w_i(t)$, synthesized for a transmitter beam with angle ϕ_0, are assembled by the receiver beamformer into the total received signal, $s_R(t)$, using the same delay as for the transmitter beamformer. However, to apply this method directly, one needs to know the target angle ϕ_0. Since, in general applications, the target angle is not known, we needs to use an inverse approach to determine it. Hence, we write the received signal as a function of the parameter ϕ_0, using the array unit delay for the direction ϕ_0 as $\Delta_0(\phi_0) = \frac{d}{c}\cos\phi_0$. (To accurately implement the time shifts when the time values fall in between the fixed values of the sampled time, we have used a spline interpolation algorithm.)

Table 1 M x M matrix of signal primitives generated in a round-robin activation of the active-sensor array elements

		Transmitters				Synthetic beamforming response
		T_0	T_1		T_{M-1}	
Receivers	R_0	$p_{0,0}(t)$	$p_{0,1}(t)$	…	$p_{0,M-1}(t)$	$w_0(t)$
	R_1	$p_{1,0}(t)$	$p_{1,1}(t)$	…	$p_{1,M-1}(t)$	$w_1(t)$
	R_2	$p_{2,0}(t)$	$p_{2,1}(t)$	…	$p_{2,M-1}(t)$	$w_2(t)$
	…	…	…	…	…	**…**
	R_{M-1}	$p_{M-1,0}(t)$	$p_{M-1,1}(t)$	…	$p_{M-1,M-1}(t)$	$w_{M-1}(t)$

A coarse estimate of the target direction is obtained by using an azimuth sweep technique, in which the beam angle, ϕ_0, is modified until the maximum received energy is attained, i.e.,

$$\max E_{\mathrm{R}}(\phi_0), \qquad E_{\mathrm{R}}(\phi_0) = \int_{t_p}^{t_p+t_0} \left|s_{\mathrm{R}}(t,\phi_0)\right|^2 dt \tag{8}$$

After a coarse estimate of the target direction is found ϕ_0, the actual round-trip time of flight, τ_{TOF}, is calculated using an optimal estimator, e.g., the cross-correlation between the receiver and the transmitter signals:

$$y(\tau) = \int_{t_p}^{t_p+t_0} s_{\mathrm{R}}(t) s_{\mathrm{T}}(t-\tau) dt \tag{9}$$

Then, the estimated $\tau_{\mathrm{TOF}} = 2R/c$ is obtained as the value of τ where $y(\tau)$ is maximum. Hence, the estimated target distance is

$$R_{exp} = c\,\tau_{\mathrm{TOF}}/2 \tag{10}$$

This algorithm works best for targets in the far field, for which the "parallel-rays" assumption holds. For targets in the near and intermediate field, a more sophisticated self-focusing algorithm, that uses triangulation principles, is used. This algorithm is an outgrowth of the passive-sensors target-localization methodologies [18]. The self-focusing algorithm modifies the delay times for each synthetic-beam response, $w_i(t)$, such that it maximizes the total response, by finding the focal point of individual responses, i.e., the common location of the defect that generated the echoes recorded at each sensor. For very close range targets, SAFT techniques [19] are utilized.

PWAS-GENERATED LAMB WAVES

The success of the EUSR concept rests on the ability of transmitting and receiving good-quality Lamb waves using the PWAS technology. Hence, considerable effort was dedicated to studying the interaction between PWAS and the thin-wall structure during the Lamb-wave generation and detection, as well as to finding the optimum excitation frequency and calibrating the Lamb wave group velocity.

Copyright © 2002 by ASME

Downloaded From: https://proceedings.asmedigitalcollection.asme.org on 06/28/2019 Terms of Use: http://www.asme.org/about-asme/terms-of-use

REVIEW OF LAMB WAVES PRINCIPLES

Lamb waves are guided waves that propagate inside thin-wall plates and shallow shells [20]. As guided-waves, Lamb waves propagate parallel to the plate mid-surface and travel at large distances with very little amplitude loss. Across the material thickness, Lamb waves present stationary wave patterns (Figure 3). Lamb waves can be either symmetric or anti-symmetric across the material thickness (S_n and A_n, respectively, where n represents the number of inflection points across the material thickness). The Lamb wave phase velocity, c_L, depends on the product between frequency, $f = \omega/2\pi$, and the material thickness, $h = 2d$. Since the wave speed varies with frequency, the propagation of Lamb waves is essentially dispersive. The dispersion curves can be obtained by solving the Rayleigh-Lamb frequency equation [21]. After defining $\xi = \sqrt{c_S^{\,2}/c_P^{\,2}}$, $\zeta = \sqrt{c_S^{\,2}/c_L^{\,2}}$, $k_L = \dfrac{\omega}{c_L}$, $q = \sqrt{k_L^{\,2} - k_P^{\,2}}$, $s = \sqrt{k_L^{\,2} - k_S^{\,2}}$, one solves, for symmetrical motion (Figure 3a) the Rayleigh-Lamb frequency equation in the form

$$\frac{\tan(\sqrt{1-\zeta^2}\,\overline{d})}{\tan\sqrt{\xi^2-\zeta^2}} + \frac{4\zeta^2\sqrt{1-\zeta^2}\sqrt{\xi^2-\zeta^2}}{(2\zeta^2-1)^2} = 0 \qquad (11)$$

Hence, the two components of the displacement can be expressed as [21]:

$$U(x,z,t) = \mathrm{Re}\left[Ak_L\left(\frac{\cosh(qz)}{\sinh(qd)} - \frac{2qs}{k_L^{\,2}+s^2}\frac{\cosh(sz)}{\sinh(sd)}\right)e^{i(k_L x-\omega t-\frac{\pi}{2})}\right] \quad (12)$$

$$W(x,z,t) = \mathrm{Re}\left[Aq\left(\frac{\sinh(qz)}{\sinh(qd)} - \frac{2k_L^{\,2}}{k_L^{\,2}+s^2}\frac{\sinh(sz)}{\sinh(sd)}\right)e^{i(k_L x-\omega t)}\right] \quad (13)$$

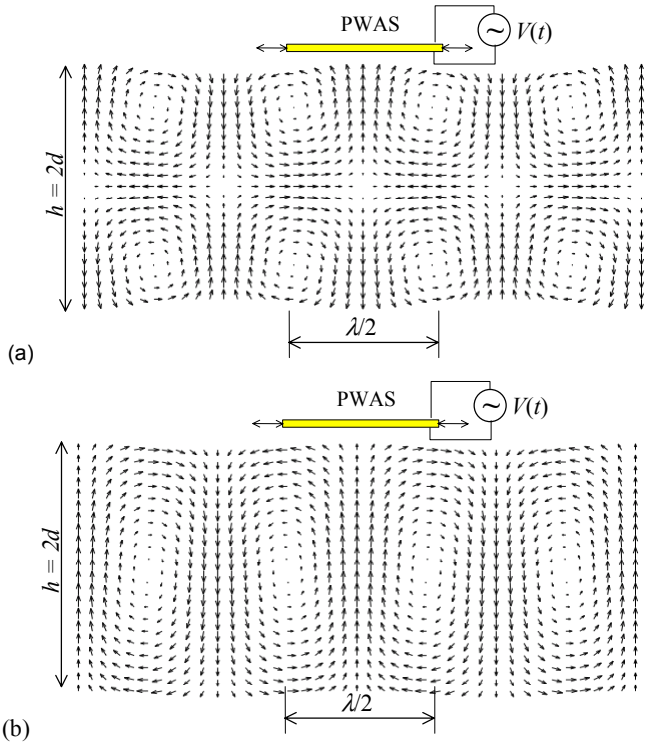

Figure 3 Simulation of Lamb wave motion in a 1-mm thick aluminum plate: (a) symmetric mode S_0, f = 1.56 MHz; (b) anti-symmetric mode A_0, f = 0.788 MHz. For full animation, see http://www.engr.sc.edu/research/lamss/default.htm

For anti-symmetric motion (Figure 3b), the Rayleigh-Lamb frequency equation becomes

$$\frac{\tan(\sqrt{1-\zeta^2}\,\overline{d})}{\tan\sqrt{\xi^2-\zeta^2}} + \frac{(2\zeta^2-1)^2}{4\zeta^2\sqrt{1-\zeta^2}\sqrt{\xi^2-\zeta^2}} = 0\,. \qquad (14)$$

and the two component of the displacement can be expressed as

$$U(x,z,t) = \mathrm{Re}\left[Ak_L\left(\frac{\cosh(qz)}{\cosh(qd)} - \frac{2qs}{k_L^{\,2}+s^2}\frac{\cosh(sz)}{\cosh(sd)}\right)e^{i(k_L x-\omega t-\frac{\pi}{2})}\right] \quad (15)$$

$$W(x,z,t) = \mathrm{Re}\left[Aq\left(\frac{\sinh(qz)}{\cosh(qd)} - \frac{2k_L^{\,2}}{k_L^{\,2}+s^2}\frac{\sinh(sz)}{\cosh(sd)}\right)e^{i(k_L x-\omega t)}\right] \quad (16)$$

The Lamb waves group velocity represents the speed with which Lamb-wave packs are sent and received along the thin-wall plate. According to Rose [3]:

$$c_g = c^2\left[c - (fd)\frac{\mathrm{d}c}{\mathrm{d}(fd)}\right]^{-1} \qquad (17)$$

where c_g is the Lamb wave group velocity, and c is the Lamb wave phase velocity. Thus, we calculated the Lamb wave group velocities dispersion curves for our specimens.

PWAS GENERATION OF LAMB WAVES

PWAS (piezoelectric-wafer active sensors) are small wafers of piezoelectric material that are permanently bonded to the material surface, and can simultaneously act as elastic-waves transmitters and receptors. PWAS are *strain transducers* that couple directly with the surface strains of the thin-wall structure. Due to the in-plane surface coupling, PWAS are ideally suited for the generation of guided plate waves (Lamb waves). Figure 3 shows how a surface mounted PWAS can simultaneously excite both axial (S_0) and flexural (A_0) Lamb waves. For efficient Lamb-wave excitation, the PWAS length, l_a, must be an integer multiple of the Lamb wave half-length, $\lambda/2$, i.e., $l_a = k\lambda/2$, k = 1, 2, … When a time-varying voltage, $V(t)$, is applied to the PWAS electrodes, the PWAS expands and contracts in accordance with the laws of piezoelectricity. Thus, the PWAS acts as a Lamb wave generator. Conversely, when a Lamb wave is present in the material under a PWAS, the surface expansions and contractions are felt by the PWAS and transformed in time-varying electric signals. In this case, the PWAS acts as a wave sensor. Of particular importance is the fact that PWAS are coupled with the material strains parallel to the material surface. Thus, transmission and reception of Lamb waves in thin-wall structures is greatly facilitated. This type of coupling, which is parallel to the material surface, is significantly more efficient for the excitation and reception of Lamb waves than that of the conventional ultrasonic transducers, which can only impinge normal to the material surface (or at an angle, when using wedge couplers). This observation, in additional to the much lower cost of PWAS transducers, highlights their advantage over conventional ultrasonic transducers in the transmission and reception of Lamb waves.

CALIBRATION OF PWAS-GENERATED LAMB WAVES

Before attempting to use PWAS in the implementation of the EUSR concept, several calibration experiments were conducted to verify that: (a) Lamb waves could be satisfactorily generated and detected with PWAS; (b) the generated Lamb waves are omnidirectional; and (c) the group velocity satisfies the theoretical predictions. Of particular interest was to prove that the amplitude of the generated waves was sufficiently strong such that perceivable echoes could be received, since the PWAS are an order of magnitude

Copyright © 2002 by ASME

Downloaded From: https://proceedings.asmedigitalcollection.asme.org on 06/28/2019 Terms of Use: http://www.asme.org/about-asme/terms-of-use

smaller and lighter than conventional ultrasonic transducers. In addition, of special interest was to prove that the Lamb waves generated by PWAS are omnidirectional, since some guided waves generated with conventional ultrasonic transducers and wedge converters were reported not to be omnidirectional, but rather confined to narrow beams [22].

A 1.6-mm thick, 2024-aluminum alloy rectangular plate (914mm x 504mm x 1.6 mm) was instrumented with eleven 7-mm sq., 0.2-mm thick piezoelectric wafers (American Piezo Ceramics Inc., APC-850). The sensors were connected with thin insulated wires to a 16-channels signal bus and two 8-pin connectors. An HP33120A signal generator was used to generate Hanning-windowed tone-burst excitation of 10-V amplitude of various frequencies and 10 Hz repetition rate. A Tektronix TDS210 two-channel digital oscilloscope, synchronized with the signal generator, was used to collect the response signals. One of the oscilloscope channels collected the signal from the transmitter PWAS, while the other channel was switched among the remaining PWAS using a digitally controlled switching unit. A National Instruments LabView™ data acquisition program was developed to control the signal switching and to download and process the data from the digital oscilloscope. To precisely determine the time of flight (TOF), the raw signals were processed using a narrow-band signal correlation followed by envelope detection. In addition, a Motorola MC68HC11 microcontroller was tested as an embedded stand-alone controlling option.

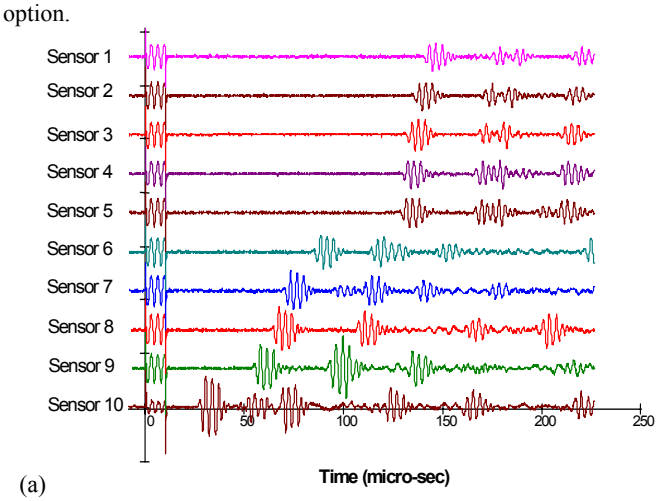

(a)

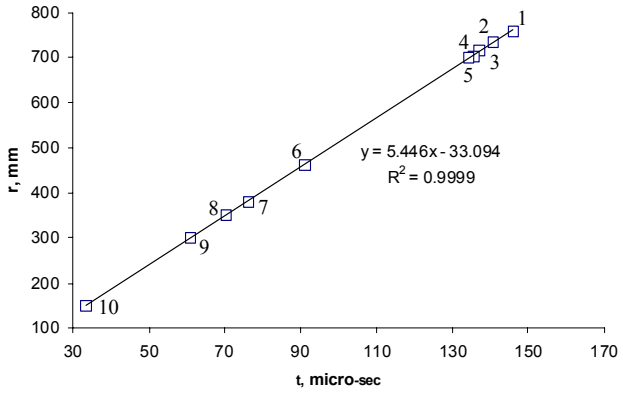

(b)

Figure 5 (a) Omnidirectionality of PWAS-generated Lamb waves: (a) reception signals on PWAS #1–10 when a constant-amplitude tone burst was applied to PWAS #11; (b) correlation between distance and time of flight.

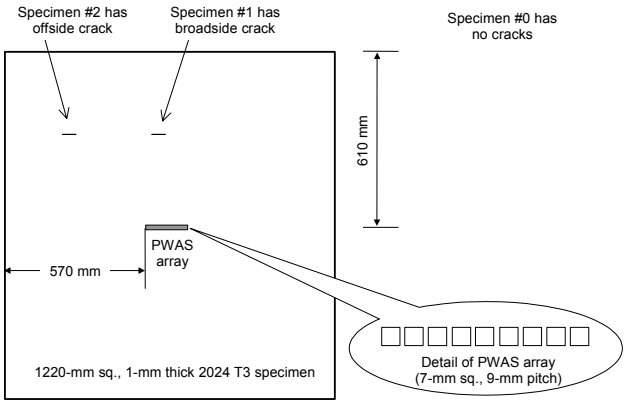

Figure 6 Thin plate specimens with 9-element PWAS array

We used PWAS #11 as transmitter and other PWAS (#1–8) as receivers. The signals observed in this investigation are shown in Figure 5a. The first row shows the signal at the transmitter PWAS #11. The initial bang and a number of echo wave packages, corresponding to the pulse-echo mode, are observable. The other rows show the signals of the PWAS receptors #1–8. The first wave package corresponds to the wave received from the transmitter PWAS, while the other wave packages are reflection from the plate edges. The time difference between the initial bang and the wave-package arrival represents the time-of-flight (TOF). The TOF is consistent with the traveled distance. Figure 5b shows the straight-line correlation between TOF and distance. The slope of this line is the experimental group velocity, c_g = 5.461 km/s. The theoretical value should be 5.440 km/s. Very good accuracy is observed (99.99% correlation; 0.4% speed detection accuracy). Thus, we have verified that: (a) Lamb waves could be satisfactorily generated and detected with PWAS; (b) the generated Lamb waves are omnidirectional; and (c) the group velocity satisfies the theoretical predictions.

EXPERIMENTAL VALIDATION

A proof-of-concept EUSR system was built in the Laboratory for Active Materials and Smart Structures (LAMSS) at the University of South Carolina to evaluate the feasibility and capability of the EUSR concept and identify the implementation issues.

EXPERIMENTAL SETUP

Three specimens were used in the experiments. These specimens were 1220-mm square panel of 1-mm thick 2024-T3 Al-clad aircraft grade sheet metal stock. One of the specimens (specimen #0) was pristine, and was used to obtain baseline data. The other two specimens were manufactured with simulated cracks. The cracks were place on a line midway between the center of the plate and its upper edge (Figure 6). The cracks were 19 mm long, 0.127 mm wide. On specimen #1, the crack was placed broadside w. r. t. the phase array, at coordinates (0, 0.305 m), i.e. at R = 305 mm, $\phi_0 = 90^0$. On the specimen #2, the crack was placed offside w. r. t. the phased array, at coordinates (-0.305 m, 0.305 m), which corresponds to R = 409 mm, $\phi_0 = 136.3^0$ w. r. t. the reference point of the PWAS array. The PWAS array was constructed from nine 7mm sq., 0.2-mm thick piezoelectric wafers (American Piezo Ceramic Inc., APC-850) placed on a straight line in the center of the plate. The sensors were spaced at pitch $d = \lambda/2$, where $\lambda = c/f$ is the wavelength of the guided wave propagating in the thin-wall structure. Since the first optimum excitation frequency for S_0 mode was 300 kHz, and the

Copyright © 2002 by ASME

Downloaded From: https://proceedings.asmedigitalcollection.asme.org on 06/28/2019 Terms of Use: http://www.asme.org/about-asme/terms-of-use

corresponding wave speed was c = 5.440 km/s, the wavelength was λ = 18 mm. Hence, the spacing in the PWAS array was selected as d = 9 mm (Figure 6).

The DAQ module consisted of an HP33120A arbitrary signal generator, a Tektronix TDS210 digital oscilloscope, and a portable PC with DAQ and GPIB interfaces. The HP33120A arbitrary signal generator was used to generate a 300 kHz Hanning-windowed tone-burst excitation with a 10 Hz repetition rate. Under the Hanning windowed tone-burst excitation, one element in the PWAS array generated a Lamb waves package that spread out into the entire plate in an omnidirectional pattern (circular wave front). The Tektronix TDS210 digital oscilloscope, synchronized with the signal generator, collected the response signals from the PWAS array. One of the oscilloscope channels was connected to the transmitter PWAS, while the other was switched among the remaining elements in the PWAS array by using a digitally controlled switching unit. A LabVIEW™ computer program was developed to digitally control the signal-switching, to record the data from the digital oscilloscope, and to generate the group of raw data files. Photographs of the experimental setup are presented in Figure 7.

Implementation of the EUSR Data Processing Algorithm

The signal-processing module reads the raw data files and process them using the EUSR algorithm. Although the EUSR algorithm is computationally non-intensive, the large amount of data points in each signal made this step time consuming. Hence, we selected to save the resulting EUSR data on the PC for later retrieval and post processing. This approach also enables other programs to access the EUSR data. Based on the EUSR algorithm, the resulting data file is a collection of signals that represent the structure response at different angles, defined by the parameter ϕ. In other words, they represent the response when EUSR scanning beam turned at incremental angles ϕ.

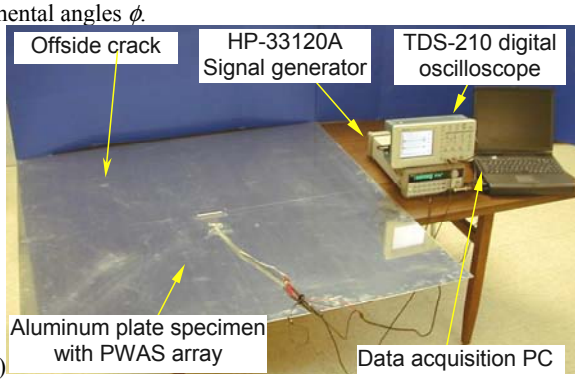

(a)

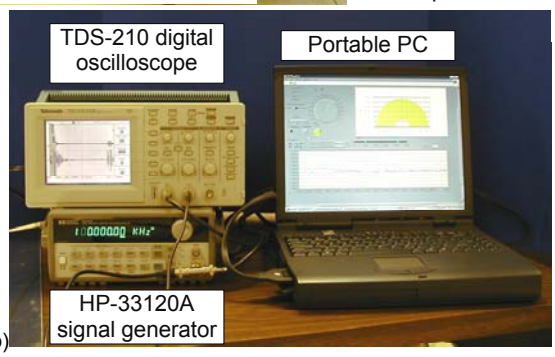

(b)

Figure 7 Experimental setup for EUSR experiment: (a) overall view showing the plate, active sensors, and instrumentation; (b) detail of the instrumentations and data acquisition

After being processed, the data was transformed from the time domain to the 2-D physical domain. Knowing the Lamb wave speed c, and using r=ct, the EUSR signal was transformed from voltage V vs. time t to voltage V vs. distance r. The signal detected at angle ϕ was plotted on a 2-D plane at angle ϕ. Since angle ϕ was stepped from 0 to180^o, at constant increments, the plots covered a half space. These plots generate a 3-D surface, which is a direct mapping of the structure being interrogated, with the z value of the 3-D surface representing the detected signal at that (x, y) location (Figure 8a). If we present the z value on a color scale, then the 3-D surface is project to the 2-D plane, and the color of each point on the plane represents the intensity of the reflections.

Experimental Results

Both the broadside crack (specimen #1) and the offside crack (specimen #2) were successfully detected. However, the offside crack presented a detection challenge since, because of the inclination of the crack with respect to the beam axis, the backscatter reflections from the crack were very faint. Figure 8b presents the EUSR signal reconstruction for the offside crack experiment.

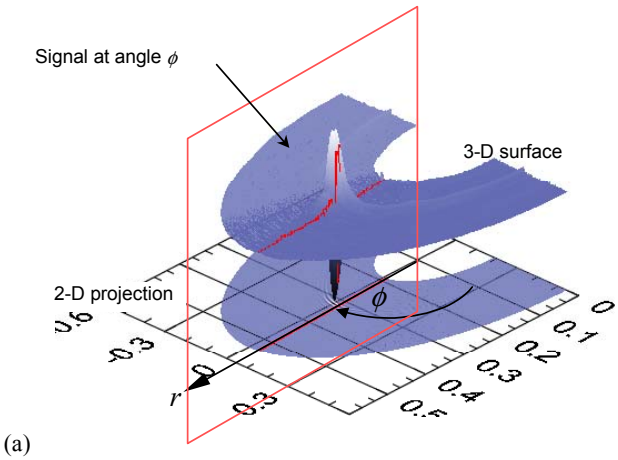

(a)

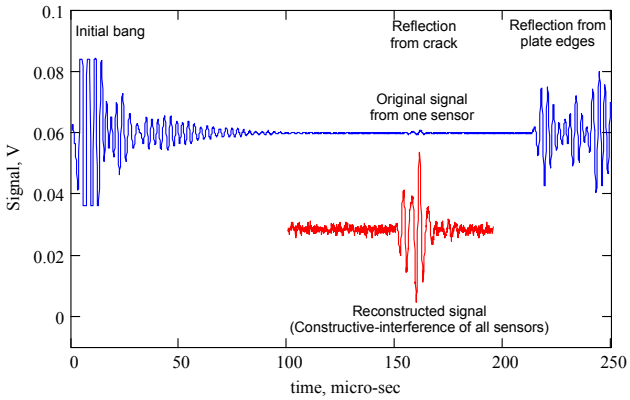

(b)

Figure 8 EUSR signal reconstruction: (a) 3-D visualization of EUSR signal reconstruction for the broadside crack specimen #1; (b) signal enhancement through the EUSR phased-array method illustrated on the offside crack specimen #2

Copyright © 2002 by ASME

Downloaded From: https://proceedings.asmedigitalcollection.asme.org on 06/28/2019 Terms of Use: http://www.asme.org/about-asme/terms-of-use

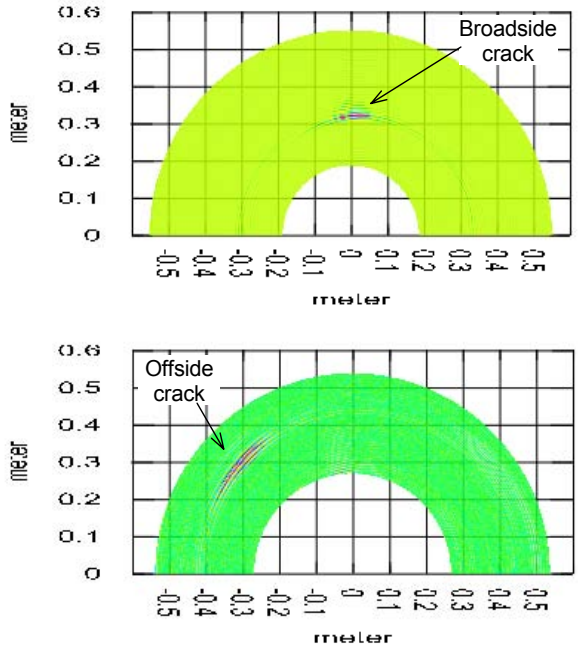

Figure 9 EUSR mapping results: (a) detection of a broadside crack (ϕ_0 = 90 deg, r = 305 mm) (b) detection of an offside crack (ϕ_0 = 136.3 deg, r = 409 mm).

The original signal (top, blue) and the reconstructed signal (bottom, red) are presented. The reconstructed signal (bottom, red) was obtained by the constructive interference of all the original sensor signals, with the appropriate time delays, as described in the section 2 of this paper. (For display purposes, the signals in Figure 8b were separated vertically by the application of a DC bias.) One notices that the original sensor signal (top, blue) displays a faint tremor at approximately 151 μs representing the backscatter reflection from the offside crack.

This tremor is very faint because the crack is positioned at such an angle that the ultrasonic interrogation beam is actually reflected away and to the left with respect to the PWAS array. What is recorded, are residual backscatter signals arriving at the sensor array. It is apparent that the signal to noise ration (SNR) of the individual sensor signal is very poor. Obviously, the original sensor signals could not be used for crack detection. However, the SNR of the reconstructed signal, as enhanced through the EUSR algorithm, is several orders of magnitude better. The enhanced signal can now be used for crack detection. In this enhanced signal, the TOF of the crack signal is easily identified as $\tau_{TOF,Offside}$ = 151 μs. Using c_g = 5.440 mm/micro-sec yields the range of the crack as $R_{Offside}$ = 411 mm. The exact value is 409 mm, i.e., 0.4% error. The accuracy of the EUSR method seems remarkable.

Figure 9 shows the EUSR detection visualization for the broadside crack (Figure 9a) and the offside crack (Figure 9b) specimens. The group velocity was used to map the EUSR data from time domain to the space domain, thus the locations of the reflectors can be visually displayed. The grids represent exact mapping in meters. The shaded area represents the swept surface. The signal amplitude is presented on color/grayscale intensity scale. The location of the crack is easily determined from the color/grayscale change. For example, Figure 9a presents the results for the broadside specimen. The small area with darker color represents high amplitude echo (reflected wave) generated when the scanning angular beam intercepted the crack. From the picture scale, we observe that this area is located at an angle of 90^0 and at approximately 0.3 m from the center of the plate. Careful analysis of the reconstructed signal yielded the exact $\tau_{TOF,Broadside}$ = 112.4 μs, corresponding to a radial position $R_{Broadside}$ = 305.7 mm. This differs a mere 0.2% from the actual position of the broadside crack on this specimen ($\phi_0 = 90^0$, R = 305 mm). The dark area in the EUSR result predicted the simulated crack perfectly. Similarly, Figure 9b presents the results for the offside specimen. It is remarkable that an echo signal could be reconstructed in spite of the fact that, because of crack orientation, the direct beam is reflected away from the EUSR array. We believe that the reconstructed signal is mainly composed of secondary backscatter generated by the crack tips. It is apparent that the offside crack is located just beyond the (-0.3 m, 0.3 m) coordinates, which compares very well with the actual values (-0.305 m, 0.305 m). The crack range $R_{Offside}$ = 411 mm, determined from the analysis of the reconstructed echo, showed 0.4% accuracy. Both Figure 8 and Figure 9 prove that the detection sensitivity and accuracy of the EUSR method is extremely good.

SUMMARY AND CONCLUSIONS

This paper has presented a novel structural health-monitoring concept – the embedded-ultrasonics structural radar (EUSR). The concept is novel because it combines the phased-array radar principles with the use of structurally-embedded arrays of piezoelectric wafer active sensors (PWAS) that can simultaneously act as transmitters and receptors of omnidirectional Lamb waves in thin-wall structures. The sensors are considered "embedded" into the structure, since they are permanently attached to the structure during its fabrication. They can be even placed inside cavities that are going to be closed up (such as wing structures), and then be left in place for the duration of the structure life. The EUSR concept opens new horizons for performing in-situ damage detection and structural health monitoring of a multitude of thin-wall structures such as aircraft, missiles, pressure vessels, oil tanks, pipelines, etc.

The systematic theoretical and experimental investigation presented in this paper has proved several essential points. First, it was shown that small (7-mm × 7-mm × 0.2 mm) PWAS could excite omnidirectional Lamb waves of sufficient amplitude for meaningful detection with conventional laboratory equipment. A frequency "sweet spot" was identified in the 300 kHz band through tuning the PWAS characteristics with the surface component of the across-the-thickness Lamb wave modeshape. It was shown that the same PWAS could be simultaneously be used as both Lamb waves transmitter and Lamb waves receiver. The captured signals were remarkably strong (up to 50 mV pp); they could be used directly in the signal-processing module without pre-amplification or other signal conditioning. It is conceivable that similar propagation will also happen in thin-gage shallow shells typical of aerospace structures. Subsequently, it was shown that the phased-array principles for transmission and reception beamforming could be successfully applied to a nine-PWAS phased array. The proof-of-concept experiments described in this paper illustrates that the EUSR concept is able to detect both broadside and offside cracks. The detection of the offside crack was particularly challenging, since the crack was oriented at an odd angle with respect to the phase-array beam, which was thus deflected away from the phased array. For this reason, in the elemental signals, the backscatter from this crack was barely noticeable. However, after the application of the signal reconstruction algorithm through the constructive interference of the signals from all the nine sensors in the phased array, the crack signal became truly "loud and clear". Remarkable

Copyright © 2002 by ASME

Downloaded From: https://proceedings.asmedigitalcollection.asme.org on 06/28/2019 Terms of Use: http://www.asme.org/about-asme/terms-of-use

detection accuracy was observed for both the broadside and the offside cracks.

The results reported in this paper indicate that the emerging field of *embedded-ultrasonics structural health monitoring* can be developed using proven phase-array ultrasonic testing methodologies that were initially designed for conventional ultrasonic transducers. The use of the small and inexpensive PWAS, instead of the relatively bulky and costly conventional ultrasonic transducers, permits the construction of embedded-ultrasonics structural health monitoring systems that can be applied to whole structures with very little weight and cost penalty. Though the active-sensor experiments reported here were conducted on simple-geometry metallic plates, the findings of this study can be easily extended to practical geometries, and to composite or hybrid-material structures.

ACKNOWLEDGMENTS

The financial support of Department of Energy through the Sandia National Laboratories, contract doc. # BF0133 is thankfully acknowledged. Sandia National Laboratories is a multi-program laboratory operated by Sandia Corporation, a Lockheed Martin Company, for the United States Department of Energy under contract DE-AC04-94AL85000.

REFERENCES

[1] Krautkramer (1998) "Emerging Technology – Guided Wave Ultrasonics", NDTnet, Vol. 3, No. 6, June 1998

[2] Rose, J. L. (1995) "Recent Advances in Guided Wave NDE", 1995 IEEE Ultrasonics Symposium, pp. 761-770

[3] Rose, J. L. (1999) Ultrasonic Waves in Solid Media, Cambridge University Press, 1999.

[4] Rose, J. L. (2001) "A Vision of Ultrasonic Guided Wave Inspection Potential", Proceeding of the 7th ASME NDE Topical Conference, NDE-Vol. 20, pp. 1-5

[5] Alleyne, D. N.; Cawley P. (1992) "Optimization of Lamb Wave Inspection Techniques", *NDTE International*, Vol. 25 (1992), No. 1, pp. 11–22

[6] Deutsch, W.A.K, Cheng, A.; Achenbach, J. D. (1998) "Defect Detection with Rayleigh and Lamb Waves Generated by a Self-Focusing Phased Array", NDT.net - December 1998, Vol. 3 No. 12, http://www.ndt.net/article/ecndt98/steel/335/335.htm

[7] Rose, J. L.; Pelts, S. P.; Quarry, M. J. (1998) "A Comb Transducer Model for Guided Wave NDE," *Ultrasonics*, Vol. 36 (1998), pp. 163–169

[8] Alleyne, D.N., Pavlakovic, B., Lowe, M.J.S., Cawley, P. (2001) "Rapid, Long Range Inspection of Chemical Plant Pipework Using Guided Waves," *Review of Progress in QNDE*, Vol. 20, (2001), pp. 180-187

[9] Wooh, S.-C.; Shi, Y. (2001) "Synthetic Phase Tuning of Guided Waves" *IEEE Transactions of Ultrasonics, Ferroelectrics, and Frequency Control*, Vol. 48, No. 1, January 2001, p. 209-223

[10] Giurgiutiu, V. (2001) *In-situ Structural Health Monitoring, Diagnostics, and Prognostics System Utilizing Thin Piezoelectric Sensors*, USC-IPMO, Disclosure ID No. 20010001 of 01/24/2001, U.S. Patent Office Application Serial No. 10/072,644 of February 8, 2002, Attorney Docket No. 16139/09021

[11] Giurgiutiu, V., Zagrai, A. N. (2001) "Embedded Self-Sensing Piezoelectric Active Sensors for On-Line Structural Identification", ASME *Journal of Vibration and Acoustics*, Vol. 124, January 2002, pp. 116-125

[12] Chang, F.-K. (1995) "Built-In Damage Diagnostics for Composite Structures", in *Proceedings of the 10th International Conference on Composite Structures (ICCM-10)*, Vol. 5, Whistler, B. C., Canada, August 14-18, 1995, pp.283-289

[13] Chang, F.-K. (1998) "Manufacturing and Design of Built-in Diagnostics for Composite Structures", *52nd Meeting of the Society for Machinery Failure Prevention Technology*, Virginia Beach, VA, March 30 – April 3, 1998.

[14] Chang, F.-K. (2001) "Structural Health Monitoring: Aerospace Assessment", *Aero Mat 2001, 12th ASM Annual Advanced Aerospace Materials and Processes Conference*, 12-13 June 2001, Long Beach CA.

[15] Giurgiutiu, V.; Bao, J.; Zhao, W. (2001) "Piezoelectric-Wafer Active-Sensor Embedded Ultrasonics in Beams and Plates", *Experimental Mechanics*, Sage Pub. (submitted August 6, 2001, log # EM 5187)

[16] Giurgiutiu, V.; Zagrai, A. N.; Bao J.; Redmond, J.; Roach, D.; Rackow, K. (2002) "Active Sensors for Health Monitoring of Aging Aerospace Structures", *International Journal of the Condition Monitoring and Diagnostic Engineering Management*, UK, Vol. 5, No. 3, August 2002 (in press)

[17] Giurgiutiu, V.; Bao, J. J. (2002) Embedded-Ultrasonics Structural Radar (EUSR) with Piezoelectric-Wafer Active Sensors (PWAS) for Wide-Area Nondestructive Evaluation of Thin-Wall Structures, USC-IPMO, Disclosure ID No. 00327 of 02/13/2002

[18] Silvia, M. T. (1987) "Time Delay Estimation", in Handbook of Digital Signal Processing, D. F. Elliot (Ed.), Academic Press, 1987

[19] Shandiz, H. T.; Gaydecki, P. (1999b) "A new SAFT Method in Ultrasonic Imaging at Very Low Frequencies by Using Pulse Echo Method", NDTnet, Vol. 4, No. 11, November 1999

[20] Lamb, H. (1917) "On Waves in an Elastic Plate", Proceedings of the Royal Society of London, Series A, Vol. 93, 1917, pp. 114

[21] Viktorov, I. A. (1967) Rayleigh and Lamb waves – Physical Theory and Applications, Plenum Press, NY, 1967.

[22] Deutsch, W.A.K, Cheng, A.; Achenbach, J. D. (1999) "Focusing of Rayleigh Waves: Simulation and Experiment", IEEE *Transactions of Ultrasonics, Ferroelectrics, and Frequency Control,* Vol. 46, No. 2, March 1999, pp. 333-340

Copyright © 2002 by ASME

Downloaded From: https://proceedings.asmedigitalcollection.asme.org on 06/28/2019 Terms of Use: http://www.asme.org/about-asme/terms-of-use